Author(s): Torsti, T. & Lindberg, V. & Puska, Martti J. & Hellsing, B.

Title: Model study of adsorbed metallic quantum dots: Na on Cu(111)

Year: 2002

Version: Final published version

Please cite the original version:

Torsti, T. & Lindberg, V. & Puska, Martti J. & Hellsing, B. 2002. Model study of adsorbed metallic quantum dots: Na on Cu(111). Physical Review B. Volume 66, Issue 23. 235420/1-10. ISSN 1550-235X (electronic). DOI: 10.1103/physrevb.66.235420.

Model study of adsorbed metallic quantum dots: Na on Cu(111)

T. Torsti,[1,2] V. Lindberg,[3] M. J. Puska,[1] and B. Hellsing[4]
[1]*Laboratory of Physics, Helsinki University of Technology, P.O. Box 1100, FIN-02015 HUT, Finland*
[2]*CSC - Scientific Computing Ltd., P.O. Box 405, FIN-02101 Espoo, Finland*
[3]*Department of Physics, Växjö University, SE-35195 Växjö, Sweden*
[4]*Department of Experimental Physics, Chalmers and Göteborg University, SE-412 96 Göteborg, Sweden*
(Received 25 July 2002; published 30 December 2002)

We model electronic properties of the second-monolayer Na adatom islands (quantum dots) on the Cu(111) surface covered homogeneously by the first Na monolayer. An axially symmetric three-dimensional jellium model, taking into account the effects due to the first Na monolayer and the Cu substrate, has been developed. The electronic structure is solved within the local-density approximation of the density-functional theory using a real-space multigrid method. The model enables the study of systems consisting of thousands of Na atoms. The results for the local density of states are compared with differential conductance (dI/dV) spectra and constant current topographs from scanning tunneling microscopy.

DOI: 10.1103/PhysRevB.66.235420 PACS number(s): 68.65.Fg, 68.37.Ef, 68.65.Hb

I. INTRODUCTION

At certain faces of metals, such as the (111) face of noble metals, the surface electron states are confined to the vicinity of the top layer by the vacuum barrier on the vacuum side and the bandgap on the substrate side.[1] The electrons in these surface states form a two-dimensional nearly-free-electron gas.[2–5] It has also been observed that when adsorbing one to several monolayers of alkali-metal atoms on these surfaces, a manifold of discrete standing-wave states, so called quantum well states, perpendicular to the surface are formed.[6,7] These states can be detected, for instance, in photoemission spectroscopy (PES),[8] inverse photoelectron spectroscopy,[9] two-photon photoemission spectroscopy[10] (2PPES) and scanning tunneling microscopy (STM).[11] A large amount of experimental data is available for the system Na on Cu(111).[6–11] The electronic structure and dynamics for this system have also been investigated by first-principles theoretical calculations.[12,13]

These localized surface states are of great interest since they play an important role in many physical processes such as epitaxial growth,[14] surface catalysis,[15,16] molecular ordering,[17] and adsorption.[18] Experimental tools such as STM and PES play an important role in the investigations, since they enable spatial and spectroscopic resolving of the electron states.

One important discovery is the confinement of surface-state electrons in so called quantum corrals. These man-made nanoscale structures are formed by deliberately assembling adatoms to enclosed structures by STM.[19] Due to the small size of the corrals, quantum effects are present, and both spatial and spectroscopic properties of the confined states can be studied experimentally. A natural way of forming low-dimensional structures on metal surfaces is by controlled growth of epitaxial layers. With an appropriate choice of deposition and annealing temperatures small islands, so called quantum dots (QD), with variable shapes and sizes may form.[20] The advantage of these structures, in comparison with the corrals, is that they are relatively stable at low temperatures. This enables the imaging and investigation of their properties without inducing structural damage. One quantum-mechanical effect of the confinement is the increase of the surface-state energy, which in turn may lead to the depopulation of the surface-state band and thereby changes in the surface properties.

In this paper, we present calculated results for the electronic structure of Na on Cu(111), with the emphasis on describing the real-space resolved density of states nearby a sodium QD adsorbed on a sodium-covered Cu(111) surface. Previously, an all-electron density-functional theory (DFT) study of a free-standing Na layer in vacuum has been presented.[21] More recently, a DFT calculation using ultrasoft pseudopotentials for the free-standing Na layer as well as for the layers adsorbed on Cu(111) have been presented.[12] A simple free-electron model calculation for a free-standing Na QD has already been published by two of the present authors.[22]

The calculations in this work are made in the context of the DFT.[23,24] More specifically, the Rayleigh-quotient multigrid (RQMG) method in axial symmetry[26,25] is used for the numerical solution of the ensuing Kohn-Sham equations. The electron-ion interaction is simplified using the jellium model,[23] where the ions are replaced by a rigid positive background charge of constant density. This model has provided basic physical understanding of the electronic structures of simple metal surfaces,[23] thin metal films,[28] vacancies and voids inside metals,[29] and finite clusters of simple metal atoms.[30] Recently, also uniform cylindrical nanowires have been studied within the jellium model.[31–33]

The paper is organized as follows: Sec. II gives a short review over experimental results for the system Na on Cu(111), Sec. III describes the computational method used in the calculations, Sec. IV discusses the details of our jellium model, and in Sec. V the results are presented and comparisons are made with experimental findings. Finally, Sec. VI gives the conclusions.

II. Na ON Cu(111)

Alkali metals adsorbed on the closed-packed (111) surface of metals form hexagonal structures at saturated monolayer

coverages, following approximately the underlying substrate structure.[34] The first monolayer of Na on Cu(111) is observed to saturate at the coverage of $\Theta = 4/9 \approx 0.44$,[35] corresponding to four Na atoms per nine surface-Cu atoms. The Na atoms, thus, form a hexagonal $(3/2 \times 3/2)$ structure and the Na atom spacing of $7.43a_0$ is comparable to the atomic distance of $6.92a_0$ in bulk Na.

The adsorption of Na atoms on the Cu(111) surface will induce a charge redistribution at the interface between the adlayer and the substrate. It has been seen from photoemission experiments[10,36] that when the Na coverage is increased, the Cu Shockley surface state decreases in energy. For coverages above $\Theta \approx 0.11$, the surface state is shifted below the lower band edge of the local band gap of the Cu(111) surface, and is no longer visible in photoemission experiments. Two-photon photoemission experiments[10] indicate other unoccupied Na-induced states in the local band gap at the Cu(111) surface, which will also decrease in energy with increasing Na coverage. For higher coverages, the lowest of these states will be downshifted below the Fermi energy, and thus get occupied. At the saturated monolayer coverage, this state will be located about 0.1 eV (Refs. 10,12, and 36) below the Fermi energy at the $\bar{\Gamma}$-point of the surface Brillouin zone. The corresponding next lowest state will be located 2.1 eV above the Fermi level[10] at the $\bar{\Gamma}$ point. The lower of the two states has one node in the z direction, while the higher has two.

If the Na-atom deposition continues after the first monolayer (ML) is completed, a second layer will start to grow. Recent STM measurements[37,38] indicate that the second monolayer of Na grows via the formation of compact islands with hexagonal atomic arrangement. Normal photoemission experiments[8,39] indicate that when the second monolayer grows the emission intensity due to one-monolayer states decreases gradually, and for coverages above 1.3 ML, a new peak ≈ 0.1 eV above the Fermi energy appears. This peak is ascribed to the two-monolayer thick parts, and the energy is shifted to somewhat lower values as the coverage is increased.

Some theoretical attention has also been paid to Na on Cu(111), including the island growth. Free-electron model calculations have been performed for circular Na (Ref. 22) as well as hexagonal Ag (Refs. 40 and 41) and Na (Ref. 42) free-standing islands. All-electron calculations for an unsupported monolayer[21] of Na and first-principles slab calculations for one-atomic-Na layer in (2×2) and $(3/2 \times 3/2)$ adsorbate structures[12] on Cu(111) have been presented. In the present paper, we report jellium model calculations for an unsupported monolayer of Na and a cylinder shaped free-standing Na QD. We also present two-density-jellium calculations for the system Na on Cu(111), where we have modeled the underlying Cu(111) substrate by using a lower-density slab to mimic the decay of the surface states into the substrate. Comparison is made with experiments and previous theoretical calculations.

III. COMPUTATIONAL METHODS

In the Kohn-Sham scheme of DFT, one solves the electron density $n(\mathbf{r})$ of the system self-consistently from a set of equations. One of these equations is the single-particle Schrödinger equation. The models used in this work are axially symmetric. Thus, the Schrödinger equation is separable, and the wave functions can be written as products,

$$\psi_{m\mathbf{k}n}(r,z,\phi) = e^{im\phi} U_{m\mathbf{k}n}(r,z). \tag{1}$$

Above, m is the azimuthal quantum number implied by the axial symmetry while n differentiates between orthogonal states with same m and $\mathbf{k}$. In the calculations involving the infinite monolayer, two $\mathbf{k}$-vectors are used as explained in Sec. IV. The external potential of the systems studied in this work is caused by the positive background charge $n_+(\mathbf{r})$. The effective potential V_{eff} includes also the Hartree potential of the electron density and the exchange-correlation potential V_{XC}, which we treat in the local-density approximation.[49] The electron density $n(\mathbf{r})$ is obtained by summing single-electron densities with the occupation numbers $f_{m\mathbf{k}n}$. The degeneracies of the states are taken into account by the factor $(2-\delta_{0m})$ and the occupation numbers $f_{m\mathbf{k}n}$ obey the Fermi-Dirac statistics with a Fermi level (E_F) so that the system is neutral. A finite temperature of 1200 K is used to stabilize the solution of the set of equations. Thus, in the present axial symmetry $[\mathbf{r}=(r,z)]$, the Kohn-Sham equations read as

$$-\frac{1}{2}\left(\frac{1}{r}\frac{\partial}{\partial r} + \frac{\partial^2}{\partial r^2} - \frac{m^2}{r^2}\frac{\partial^2}{\partial z^2} + 2V_{eff}\right) U_{m\mathbf{k}n}(\mathbf{r}) = \varepsilon_{m\mathbf{k}n} U_{m\mathbf{k}n}(\mathbf{r}) \tag{2}$$

$$n(\mathbf{r}) = 2\sum_{m\mathbf{k}n} (2-\delta_{0m}) f_{m\mathbf{k}n} |U_{m\mathbf{k}n}(\mathbf{r})|^2, \tag{3}$$

$$V_{\text{eff}}(\mathbf{r}) = \Phi(\mathbf{r}) + V_{\text{XC}}(\mathbf{r}), \tag{4}$$

$$\left(\frac{1}{r}\frac{\partial}{\partial r} + \frac{\partial^2}{\partial r^2} + \frac{\partial^2}{\partial z^2}\right)\Phi = -4\pi[n_-(\mathbf{r}) - n_+(\mathbf{r})]. \tag{5}$$

The Schrödinger equation (2) is solved using the RQMG method,[26] which has been implemented in various geometries, including the axial symmetry.[26,25] In the RQMG method, the Rayleigh quotient $\langle\psi|H|\psi\rangle/\langle\psi|\psi\rangle$ on the finest level grid is directly minimized, the orthogonality constraint being taken into account by a penalty functional. The Poisson equation (5) is solved for the electrostatic potential $\Phi(\mathbf{r})$ using a standard multigrid method.[43]

To obtain self-consistency, we use the simplest possible potential mixing scheme,

$$V_{in}^{i+1} = AV_{out}^{i} + (1-A)V_{in}^{i}. \tag{6}$$

The largest system of this work contains 2550 electrons, the diameter of the supercell being 170 Å. Obtaining self-consistency in such a system requires a very small A value of 0.005. Otherwise, the charge sloshing results in divergence. More sophisticated mixing strategies[27] will be indispensable in the future calculations. However, because of the simplicity of our model systems, we can very accurately estimate an

initial guess for the self-consistent effective potential of large systems using the more easily convergent smaller systems as reference.

In our largest calculation, a grid of 319×95 points is used for the presentation of the wave functions, potential, and density. Taking into account the unoccupied states needed in the modeling, up to 2400 different states have to be solved at every self-consistency iteration. Luckily, it is straightforward to parallelize the calculation over the 65 different m values and the two **k** points (see below). Moreover, the RQMG method[26] handles this part of the calculation with optimal efficiency.

The two-jellium model for the surface described in Sec. IV results in an asymmetric density distribution with a surface dipole. Thus, the electrostatic potential on the substrate side is a constant different from that on the vacuum side. For the Poisson equation, we thus use the boundary condition of zero derivative on the substrate side, and that of zero value on the vacuum side. Solving the Poisson equation, the boundaries above and below the system are extended to a distance five times greater than in the case of the wave functions.

In this work, we calculate the local density of states (LDOS) above a surface at distances corresponding to those typical in STM measurements (of the order of $20a_0$). At such distances, the amplitude of the wave function decreases by several orders of magnitude. This kind of modeling is thus a serious test for the RQMG method. We have checked the accuracy of our method for the spherical harmonic oscillator and a model hydrogen atom potential, for which the wave-functions are known analytically. The evanescent tails of the wave functions solved with the RQMG method agree with the analytical ones, even when the amplitude of the wave functions has dropped by 20 orders of magnitude. This level of accuracy is beyond the reach of plane-wave methods, where periodic boundary conditions are necessary, and which provide a uniform accuracy across the calculation volume, resulting in spurious oscillations in the vacuum parts of the system.

IV. MODELING THE SYSTEM

We are interested in the system of a monolayer-thick Na QD on the complete Na monolayer on the Cu(111) surface. We know from experiments that these islands are approximately hexagonal in shape, following the underlying structure of the Na monolayer.

In order to interpret recent STM data for these types of systems, mapping the energy resolved real-space electron density near a QD is necessary. First, it is of interest to find what level of theoretical modeling is required. It has been shown previously[40–42] that simple two-dimensional ''particle-in-a-box'' calculations give qualitatively good results, in the sense that the peak structure of LDOS resembles spectra obtained in the STM dI/dV measurements. In this work, we improve the theoretical description by performing self-consistent three-dimensional DFT calculations, where the effects of the underlying monolayer and substrate are introduced. The hexagonal QD is modeled by a cylindrical jellium QD, and the underlying Na monolayer and Cu(111) substrate by the two-density-jellium slab, as described below. Comparisons between calculations of free-standing QD's and QD's on a substrate show indeed that the underlying monolayer and substrate induce a new type of states that the simple particle-in-a-box calculations cannot account for. Since the z dependence of wave functions is included in our calculations, we can calculate the tunneling current at realistic STM-tip distances above the system, and estimate the energy dependence of the step height from the calculated constant current topographs.

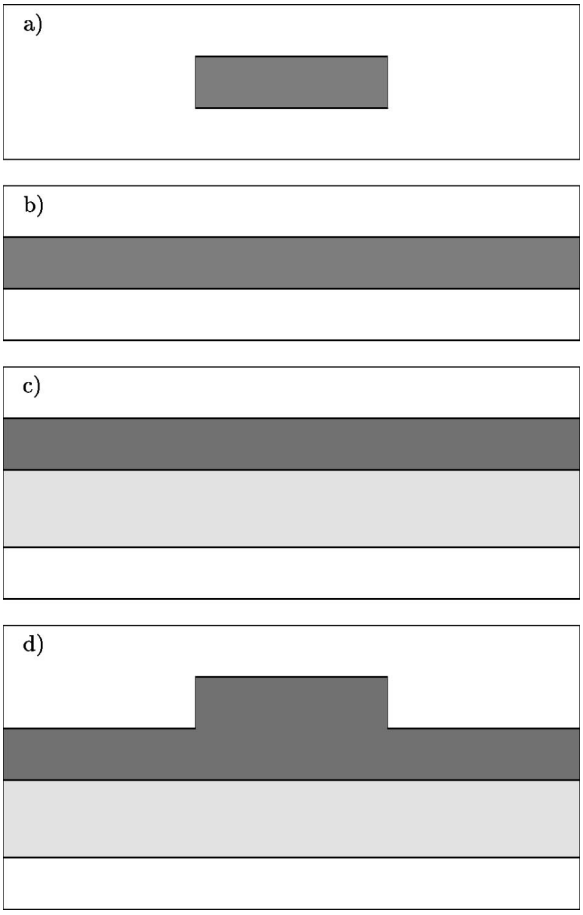

FIG. 1. Profile of the axially symmetric background charge in the case of (a) jellium model for free-standing Na quantum dot (b) jellium model for free-standing Na monolayer (c) two-jellium model for Na monolayer on Cu(111) (d) two-jellium model for Na quantum dot on Na monolayer on Cu(111)

The different model systems studied in this work are shown in Fig. 1. Our model is readily applicable to the case of a free-standing cylindrical quantum dot, where we use zero Dirichlet boundary conditions for the wave functions and for the Coulomb potential. The next step is to model a free-standing monolayer. A uniform planar system cannot be exactly reproduced in the axial symmetry. We adopt an approximation scheme analogous to the Wigner-Seitz method.[44] We imagine the plane being filled by hexagons, and then approximate these hexagons by area-covering circles. In order to sample the Brillouin-zone of the lattice of circles we use two **k**-points, $\mathbf{k}=0$ and **k** at the Brillouin-zone

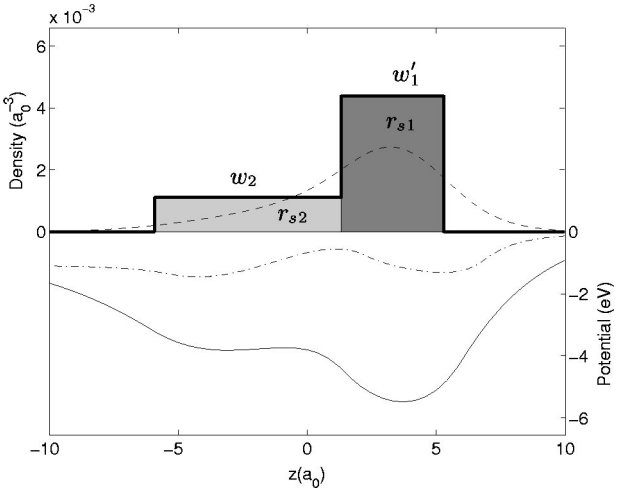

FIG. 2. One complete monolayer of Na on Cu(111) surface within the two-jellium model. The positive background charge (shaded areas), electron density (dashed line), effective potential (solid line), and electrostatic potential (dash-dotted line) are shown. The shading corresponds to Fig. 1.

boundary. The wave functions with $\mathbf{k}=0$ are required to have a vanishing radial derivative at the radius of the circle, whereas the wave functions with $\mathbf{k}$ at the Brillouin-zone boundary vanish there. According to our calculations, the model gives a uniform (r independent) charge distribution for the monolayer. It also minimizes the interactions between a QD inside a circle with its periodic images.[45]

The next step is to place the Na monolayer on top of the Cu(111) substrate. The effect of the substrate is modeled using the *two-jellium model*, which is illustrated in Figs. 1(c) and 2. We do not model the electrons of the bulk Cu. The density of electrons per unit area in the two-jellium model is kept the same as in the jellium model for a free-standing monolayer. We add a layer of lower-density jellium, in order to mimic the different wave-function decays into the substrate and into the vacuum. The thickness w_2 and density (via r_{s2}) give two free parameters of the lower-density jellium, which we adjust in order to reproduce the relevant experimental values of the first and second surface band bottoms at the coverages of 1 ML and 2 ML, respectively. Here the first and second bands correspond to wave functions with one and two nodes in the vertical direction, respectively. The thickness w_1' of the higher-density jellium in the two-jellium model is given by

$$w_1' = w_1 - \left(\frac{r_{s1}}{r_{s2}}\right)^3 w_2, \tag{7}$$

where w_1 is the thickness of the free-standing Na monolayer.

A. The underlying monolayer and substrate

To test our model, we first study the systems of a free-standing Na monolayer and that of a Na monolayer on Cu(111), and compare the results with other theoretical results and experimental findings. The Na jellium density is determined from the bulk nearest-neighbor distance of $6.92a_0$ and the experimental height of $5.5a_0$ (2.9 Å) of 1 ML of Na on Cu(111).[38,42] The resulting density parameter $r_s = 3.79a_0$ gives a slightly higher density than its bulk value of $3.93a_0$ for Na. The thickness and the density of the lower-density slab have been chosen by fitting the bottom of the second band for the 1-ML-Na coverage and that of the third band for the 2-ML-Na coverage on Cu(111) to the experimental values.[10,36,39] The values of $r_{s2}=6.0a_0$ and $w_2 = 6.3a_0$ give (using the unit cell of radius $72.8a_0$ containing 400 electrons per monolayer) in the 1-ML case the bottom of the second band at 75 meV below the Fermi level and in the 2-ML case, the bottom of the third band at 50 meV above the Fermi level. These values are reasonably close to the experimental values of about 100 meV below and above the Fermi level, respectively.[8,36,39] The correct positions relative to the Fermi level are important because we solve for the electronic structures self-consistently, so that the occupancies of the single-electron states affect the potential and the character of the states themselves.

B. The quantum dot

We start by studying a free-standing monolayer-thick Na QD [Fig. 1(a)], since this system shows close resemblance to the simple particle-in-a-box system often used as a first approximation when describing the electronic structure of a QD on a surface. The number of atoms in the QD is chosen to 100, which corresponds to a QD radius of about $R = 36.40a_0$. The uppermost panel in Fig. 3 shows the corresponding energy spectrum relative to the Fermi energy E_F. Note that the the discrete energy eigenvalues are plotted as a function of the quantum number m and not as a function of $\mathbf{k}$. There are three bands below the vacuum level, but only the first band (no horizontal nodal planes) is occupied. The emergence of the succeeding second and third bands can be seen as the condensation of the energy levels at around 1.1 eV and 2.5 eV, respectively.

The LDOS calculated at the cylinder axis at the jellium edge and at $8a_0$ above the edge are shown in the lowest and the middle panel of Fig. 3, respectively. Only states with $m = 0$ contribute, since they are the only ones with nonzero contributions at the axis. The discrete energy levels are broadened to Lorenzians with the width $\Gamma = 8$ meV. The LDOS at the jellium edge can easily be resolved in terms of the contributions from the different bands: The peaks corresponding to first, second, and third bands form series with quadratically increasing intervals and smoothly increasing peak amplitudes. At the distance of $8a_0$ above the QD, the contribution due to the first-band states is diminished and the contribution due to the third-band states with high quantization in the z direction (two horizontal nodal planes) is dominating the LDOS. Comparison with the results of the simple particle-in-a-box calculation by Lindberg and Hellsing[22] shows that these two calculations give qualitatively the same results.

We now compare these results for the free-standing QD to the system of the QD adsorbed on a Na monolayer on the Cu(111) surface [Fig. 1(d)]. In our calculation, the substrate is a two-jellium cylindrical supercell containing 400 elec-

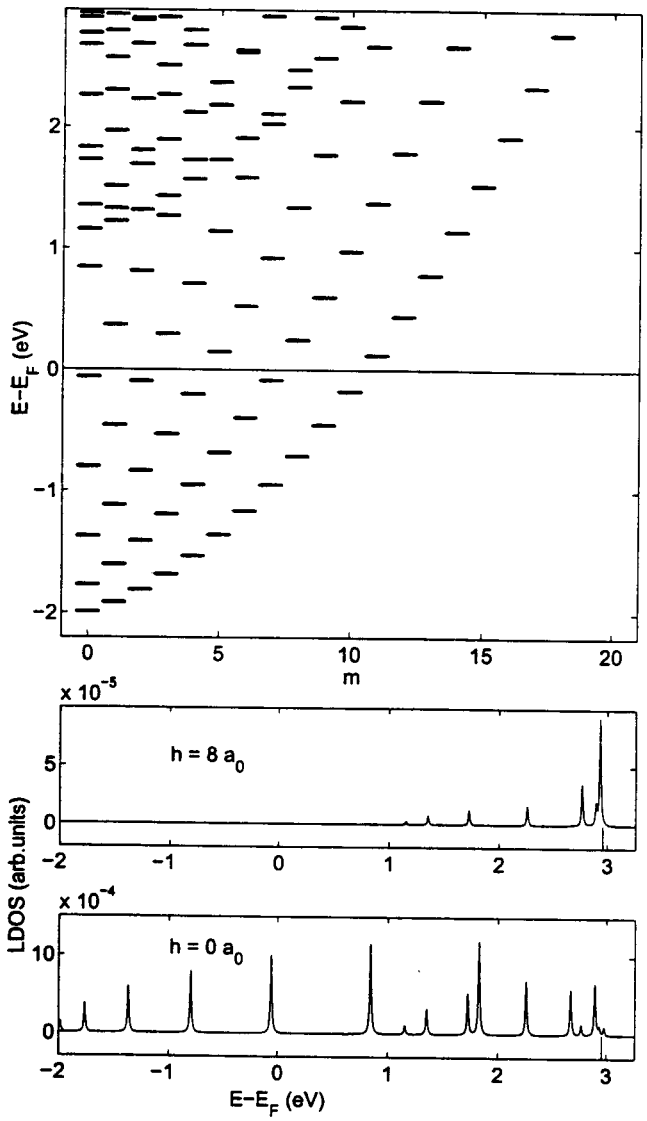

FIG. 3. The uppermost panel: Energy spectrum of the free-standing cylindrical jellium QD [Fig. 1(a)] containing 100 electrons. The discrete eigenenergies are shown as a function of the quantum number m. The top of the figure corresponds to the vacuum level. The middle panel: The LDOS calculated at the cylinder axis at $8a_0$ above the jellium edge. The lowest panel: The LDOS calculated at the cylinder axis at the jellium edge.

trons. The energy spectrum is shown in the uppermost panel of Fig. 4, in which the different m levels corresponding to the $\mathbf{k}=0$ points are given with the $\mathbf{k}$ dispersion calculated using the $\mathbf{k}$ point at the Brillouin zone boundary. In comparison with the spectrum of the monolayer-thick QD in Fig. 3, the bands are shifted downwards because of the larger jellium thickness at the QD. The lowest-energy states (in the bulb of the level diagram) have no $\mathbf{k}$-dispersion and they are localized at the QD and the substrate slab below it (see Fig. 5). Their dispersion as a function of m is similar to that in Fig. 3. Introducing the underlying substrate gives rise to a new type of states, which are not localized to the QD region. In fact, these states form the overwhelming majority. As a result, new bands are induced in the energy spectrum and they are less dispersive as a function of m. The reduced m dispersion reflects the fact that the states are extended over the entire circular supercell. For the same reason, these bands have a larger dispersion in the $\mathbf{k}$ space than the localized QD bands. A simple particle-in-a-box or free-standing QD calculation cannot provide states of this kind, and it is, therefore, interesting to see up to what extent they contribute to the local electronic structure above the QD.

The LDOS for the QD adsorbed on a Na monolayer on the Cu(111) surface is given in the lowest and the middle panels of Fig. 4 at the jellium edge and at $14a_0$ above the edge, respectively. In order to avoid complications due to the interactions between the supercells, we calculate the LDOS using only the $\mathbf{k}=0$ states and the LDOS is then calculated as in the case of the free-standing monolayer-thick Na QD. To enable a thorough comparison with the free-standing QD results, we have to study first the wave functions in more detail.

Figure 5 gives all the wave functions in the interesting energy region for the $m=0$ states of the QD adsorbed on the Na monolayer. The first three states, $n=1,2,$ and 3, correspond to states within the first band. They are localized to the QD and the substrate slab below it and they have no nodes in the z direction. The $n=4$ state shows another character with a density no longer localized to the QD region but spreads also to the slab region around. This is the first state belonging to the new type of bands induced by the slab. State $n=8$ is the beginning of the next band consisting of states with one node in the z direction (second band in the QD). These states are resonance states, the amplitude of which is strongly enhanced in the QD region, but due to the hybridization with the delocalized slab states they are actually delocalized to the whole system. The $n=14$ state starts the next band consisting of delocalized states with one horizontal node in the slab region, i.e., it is a second band in the slab. Finally, state $n=16$ represents the first-resonance state with two nodes in the z direction (third band in the QD). In Fig. 5, one notes that the states $n=16$ and 17 and also the states $n=19$ and 20 form pairs. The state lower in energy in the pair is a bonding combination of a QD state and a surrounding slab state, whereas the state higher in energy is an antibonding combination.

The electronic structure of the QD adsorbed on the Na monolayer, discussed above in terms of the $m=0$ wave functions, is reflected in the LDOS in Fig. 4. First, in the LDOS at the jellium edge, we notice that in comparison with the free-standing QD model, the underlying slab introduces a new type of bands and squeezes the other bands more tightly together to fit more states below the Fermi level (the lowest panels of Figs. 3 and 4). Therefore, the present LDOS looks qualitatively different from that of the monolayer-thick unsupported QD in Fig. 3. Moreover, the hybridization of the QD and surrounding slab states to bonding-antibonding pairs causes the splitting of peaks seen clearly for the third-band states at the distance of $14a_0$ above the jellium edge (the middle panel of Fig. 4). If we had a continuous spectrum of slab states, we would have a single resonance peak with a finite energy width.

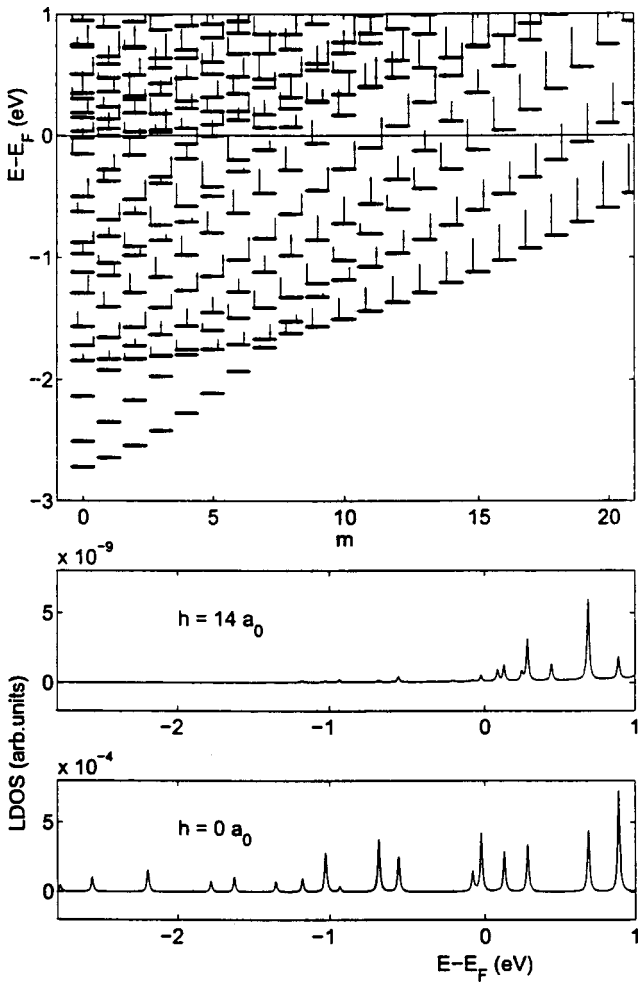

FIG. 4. The uppermost panel: Energy spectrum of the system of a QD containing 100 electrons on top of a two-density-jellium slab described by a supercell of 400 electrons [Fig. 1(d)]. The $\mathbf{k}=0$ eigenenergies are given by thick horizontal bars. The thin vertical bars indicate the dispersion in the **k**-space. The middle panel: LDOS calculated at the cylinder axis at $14a_0$ above the jellium edge. The lowest panel: LDOS calculated at the cylinder axis at the jellium edge.

Having the modeling of the STM results in mind, the interesting question arising is whether or not the localized states calculated by the free-standing QD model give the same LDOS far above the QD as the states in the model including the substrate slab. Studying the LDOS plots, matching each peak with the corresponding wave function, we notice that the resonance states with strongly enhanced amplitude in the QD region are dominant at large distances above the QD. The contribution of the more delocalized slab states is small. Therefore, the free-standing QD model is expected to preserve validity in predicting LDOS at large distances above the QD. The too broad energy spectrum in the free-standing QD model can be corrected for by increasing the dot height with a monolayer of Na jellium or with a two-jellium layer.

V. COMPARISON WITH EXPERIMENT

One of the most useful instruments in surface science is the scanning tunneling microscope (STM).[46,47] It can be used for measuring the real-space electronic distribution with atomic resolution, as well as the local energy distribution of electrons and the lifetimes of excited electron states. The real-space distribution is achieved when scanning the surface either in the constant current mode, where the tunneling current is kept constant by changing the tip-surface distance using a feedback mechanism, or in the constant height mode, where the tunneling current is measured when scanning the surface at a constant tip height. The resulting image then displays the topography of the surface. Information about the local electronic structure is obtained by measuring the current variation with the applied voltage. This quantity, the differential conductance dI/dV, is proportional to the product of the local density of states (LDOS) and the transmission coefficient T.[48,50] However, if the applied voltage is small, the bias dependence of T is small, and with Eq. 3, we approximately have

$$\frac{dI}{dV} \propto \sum_{m\mathbf{kn}} (2-\delta_{0m}) |U_{m\mathbf{kn}}(\mathbf{r})|^2 \delta(\epsilon_{m\mathbf{kn}} - eV). \qquad (8)$$

In the STM study by Kliewer and Berndt,[42] constant current topographs and dI/dV measurements are presented for a Na island on Na monolayer on Cu(111). The size of the island is $230\times170a_0^2$ (120×90 Å^2). We have studied a cylindrical jellium dot with similar dimensions, i.e., having the radius of $85a_0$ and containing thus about 550 electrons. The Na/Cu substrate is described in our calculations by a cylindrical two-density-jellium supercell with the radius of $160a_0$ and containing 2000 electrons. The radius of $85a_0$ is actually fixed to reproduce the peak structure of dI/dV spectra by Kliewer and Berndt[42] as well as possible (See Fig. 6 and discussion below). For comparison, Kliewer and Berndt[42] used in their modeling two-dimensional hard-wall hexagons with the radius of $83a_0$.

We show in Fig. 6 the LDOS at $18a_0$ above the jellium edge, both at the z axis of the QD, and at $r=20a_0$ away from the axis. The height corresponds to a typical tip-sample distance in the STM experiments. The LDOS is calculated as for the smaller systems in Sec. IV B. The peaks in the figure correspond to states with two horizontal nodes in the 2-ML part of the system (third band in the QD). At the axis, only the $m=0$ states contribute, while away from the axis also peaks with $m\neq0$ occur. The LDOS peaks can be labeled with the ''quantum number'' N by counting for the number of radial nodes of the corresponding wave functions in the 2-ML part (See Fig. 6). For $m=0$, the $N=1$ state has no radial nodes in the dot region, whereas $N=2$ has one radial node and so on for larger N. As in the case of the smaller dot discussed above in Sec. IV B, the states strongly peaked in the QD are resonance states due to the hybridization with the states of the surrounding monolayer and span the whole system. Besides the delocalization of the states, the resonance character causes the fact that in the LDOS (Fig. 6), several

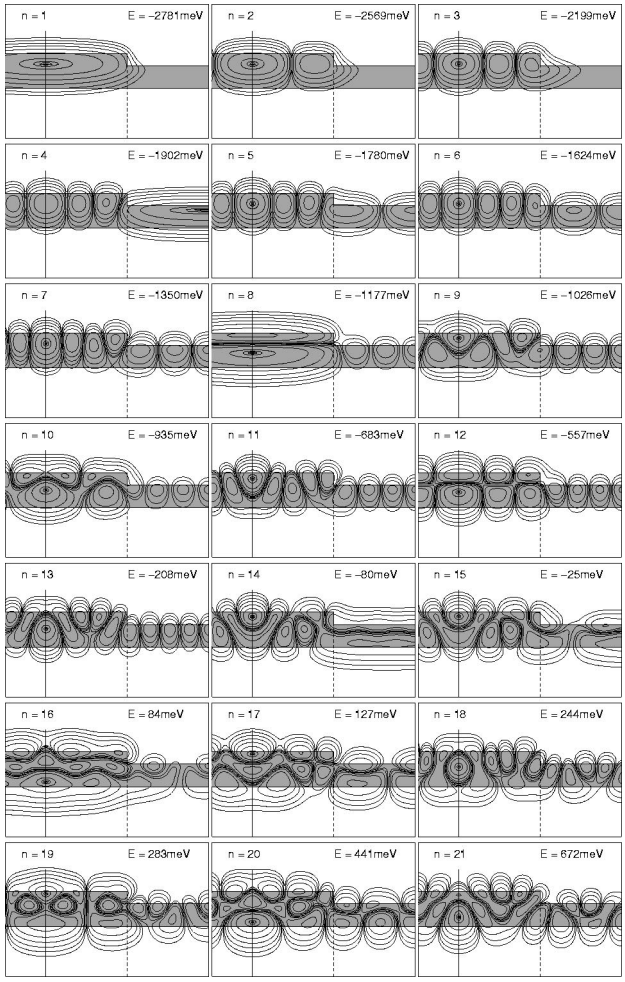

FIG. 5. Wave functions for the 21 lowest lying $m=0$, $\mathbf{k}=0$ states for the system of a monolayer-thick QD, containing 100 electrons, on top of a Na/Cu slab (400 electrons per supercell). The wave functions are plotted in a plane parallel to the z axis through the center of the QD. In each subfigure, the cylinder axis is shown by the solid vertical line. The shading indicates the positive background charge and the dashed vertical line points its QD edge. The upper, lower and right-hand subfigure borders and the cylinder axis limit the computation volume with the dimension of $(73\times 60)a_0^2$.

peaks may correspond to the same resonance state as discussed earlier for the smaller system. We have identified the LDOS peaks by examining the wave functions. The horizontal lines below the quantum numbers m and N connect the peaks belonging to the resonance in question.

The relative positions of peaks appearing in the experimental dI/dV spectra by Kliewer and Berndt[42] are shown in Fig. 6 as arrows pointing downwards. The experimental data is shifted so that the lowest experimental peak coincides with the lowest calculated peak. The experimental spectrum is recorded slightly off from the center of the hexagonal QD, which should be taken into account when comparing with the calculated results. Previous two-dimensional free-electron calculations for hexagonal potential boxes have reproduced well the experimental peak positions.[41,42] In the present modeling, the experimental peak positions agree with the calculated $m=0$ resonance positions with the exception of the

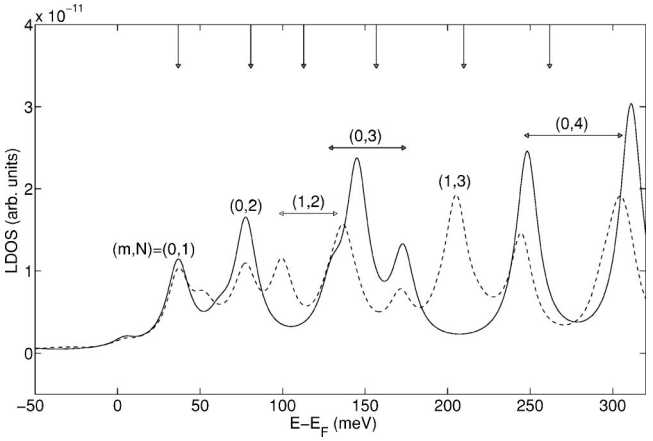

FIG. 6. Cylindrical QD containing 550 electrons on two-jellium substrate. The local density of states is shown at $18a_0$ above jellium edge at the axis (solid line) and at $r=20a_0$ (dashed line) away from the axis. Lorenz broadening with $\Gamma=8$ meV has been used. The relative experimental peak positions[42] are given by vertical arrows pointing downwards. The peaks are identified with (m,N) resonance states having two horizontal node planes in the QD.

third and fifth experimental peak. The calculated $m=0$ resonances obey the pattern $\varepsilon_n=E_0+AN^2$ as would be expected for a free particle in a hard-wall cylinder. We have fitted $E_0\approx 22$ meV, $A\approx 15$ meV. It is gratifying to note that in the LDOS recorded off the cylinder axis, strong $m=1$ resonance peaks appear so that the third and fifth experimental peaks can be explained. Thus, our model can reproduce quantitatively the experimental peak positions. According to our calculations, the resonance width increases toward higher energies. The increase is maybe slightly stronger than in experiment, indicating a somewhat too weak confinement of the resonance states in our model.

We have also calculated the isosurfaces of the LDOS at the energies corresponding to the dominant peaks in Fig. 6. The results are shown along with the total electron density in Fig. 7. In order to see clearly the nodal structures of the different states, the LDOS is calculated using a smaller Lorenzian width of 0.8 meV. The density is smooth in the interior of the QD and shows minor oscillations at the perimeter of the QD. The development of the nodal structure is clear and compares qualitatively well with that found in the experimental dI/dV maps.[38] It can also be seen that the isosurfaces corresponding to the two $(m,N)=(0,4)$ peaks differ from each other mainly near the perimeter of the dot. The higher peak shown at the energy corresponding to the highest (0,3) state, on the other hand, does not show equally clear (0,3) character. The explanation is the appearance of a state with quantum numbers (2,2) at almost exactly the same energy.

From Eq. (8), we obtain a simple formula for the tunneling current

$$I(U,r,z)\propto\int_{E_F}^{E_F+U}\rho(E,r,z)dE, \tag{9}$$

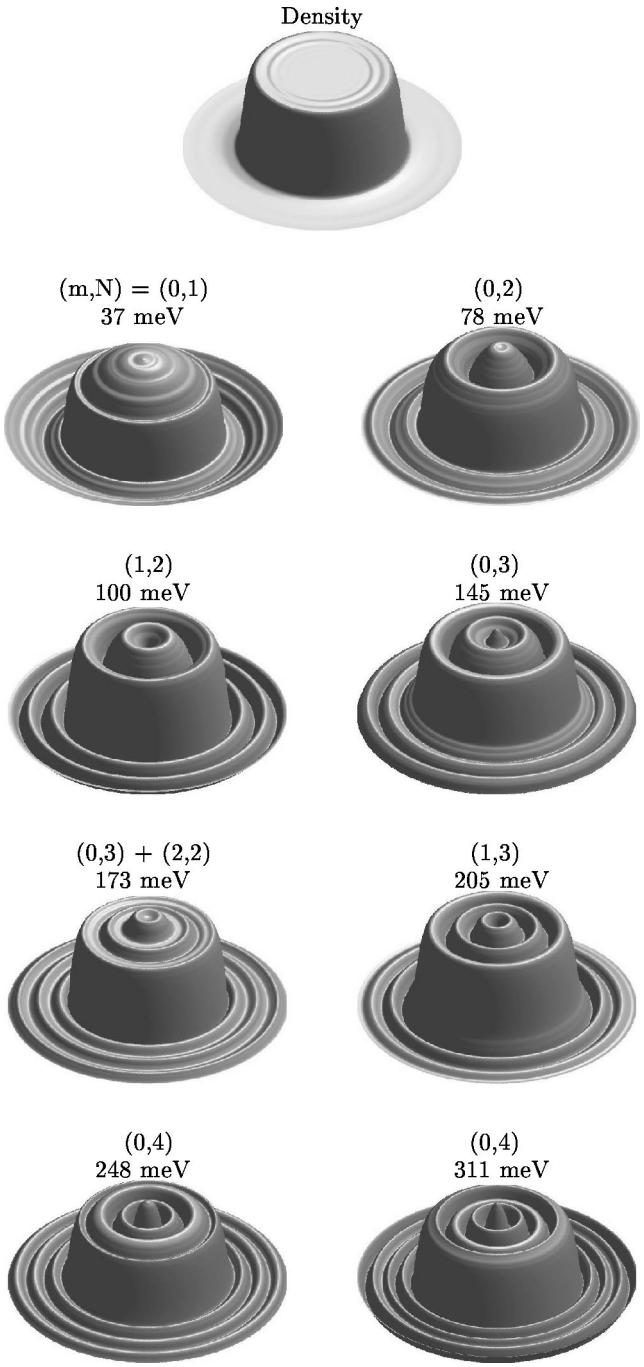

FIG. 7. Cylindrical QD of 550 electrons on two-jellium substrate. Isosurfaces of the electron density (top) and the LDOS (with $\Gamma = 0.8$ meV) at energies corresponding to the dominant peaks of Fig. 6. The quantum numbers of the dominant states contributing at each energy is indicated. The isovalue for each plot is chosen as the value of the corresponding quantity at $18a_0$ above the jellium edge and $30a_0$ off from the axis. The height-to-radius ratio in the plots is exaggerated.

where $\rho(E,r,z)$ is the LDOS at the height z and distance r from the axis. Calculated isosurfaces of this quantity form numerical constant current topographs, from which we can estimate the apparent step height at the perimeter of the QD.

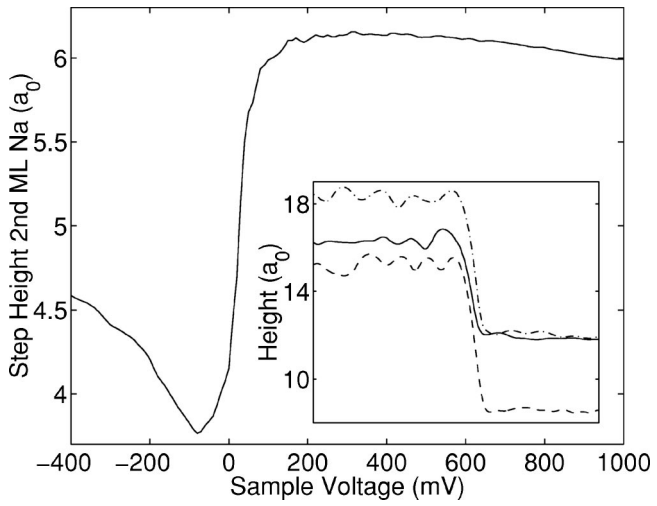

FIG. 8. Cylindrical QD containing 550 electrons on two-jellium substrate. The step height of the second Na monolayer determined from calculated constant current surfaces [Eq. (9)] is shown as a function of the bias voltage (energy relative to the Fermi level). The inset shows the LDOS isosurface profiles (height-to-radius ratio exaggerated) at energies -400 meV, (dashed line) 0 meV (solid line), and 400 meV (dash-dotted line). The height is measured from the jellium edge of the second-ML QD. The width of the plotted region is $160a_0$, i.e., the radius of the circular supercell.

The inset of Fig. 8 shows the constant LDOS height as a function of the distance from the cylinder axis for the bias voltages of -400, 0, and $+400$ meV. The value of LDOS is 10^{-11} arbitrary units on the scale of Fig. 6. The absolute height of the isosurface from the jellium edge depends naturally on the LDOS value chosen but according to our calculations, the relative changes are insensitive to the LDOS value over a wide range of values. In order to construct the apparent step height, we first obtain the numerical constant current topographs [Eq. (9)], then average the profiles over the oscillations above the 2-ML and 1-ML parts of the system and take the difference. The results are shown in Fig. 8 as a function of the bias voltage. The trends seen can be explained by studying the LDOS isosurfaces (see the inset of Fig. 8), and then noting that the constant current surfaces are obtained by simple integation [Eq. (9)]. At -100 meV, the second band starts to contribute in the 1-ML part of the system raising the height there and thereby lowering the step height. Then the onset of the third band in the 2-ML part raises the step again. This rise is similar to that seen in the experiment by Kliewer and Berndt[38] as well as the decline at higher voltages. However, the comparison with the experimental result shows differences: our step height is too low by a factor of 2, and the raising of the step at negative bias voltages is not seen in the experiment. There may be several reasons for the differences in the step heights. One is that the experimental step height of $5.5a_0$ (2.9 Å), which is determined at a voltage just before the rise in the step height is directly used as the thickness of the jellium describing the second monolayer of Na. A more consistent procedure might be to take the voltage dependence into account. Moreover, the apparent step height depends on the

relative vacuum decay rates of the second and third-band states of the 1-ML and 2-ML systems, respectively. Their correct description may be too demanding for our simple model.

VI. CONCLUSIONS

In this paper, we have presented a model for the electronic structures of alkali-metal islands or quantum dots adsorbed on metal surfaces. In particular, we have focused on the system of Na on the Cu(111) surface, where approximately hexagonal Na quantum dots have been observed to form during the epitaxial growth of the second-Na monolayer.

We have modeled the quantum dots as small cylindrical jellium islands, and the underlying Na monolayer and Cu substrate as a two-density-jellium slab. The parameters of the model have been chosen to fit experimental spectroscopic data and calculated first-principles band structures for one and two completed monolayers of Na on the Cu(111) surface. The calculations were performed in the context of the density-functional theory using a real-space electronic structure calculation method.

The calculated results are compared with experimental findings from scanning tunneling microscope and photoemission experiments. The model gives local densities of states, which are in a quantitative agreement with constant current topographs and dI/dV spectra and maps. Thereby, the idea of surface states, which are localized as resonances at the quantum dots is supported. The future applications of the model will include studies of the adsorption and dissociation of molecules in the vicinity of alkali-metal quantum dots.

ACKNOWLEDGMENTS

We would like to thank Lars Walldén and S. Å. Lindgren for sharing their knowledge on the system based on PES experiments. We would like to thank R.M. Nieminen for many useful discussions. We acknowledge the generous computer resources from the Center for Scientific Computing, Espoo, Finland. One of the authors (T.T.) acknowledges financial support by the Vilho, Yrjö and Kalle Väisälä foundation. This research has been supported by the Academy of Finland through its Centers of Excellence Program (2000–2005).

[1] H. Lüth, *Surfaces and Interfaces of Solids* (Springer-Verlag, Berlin, 1993).
[2] P.O. Gartland and B.J. Slagsvold, Phys. Rev. B **12**, 4047 (1975).
[3] P. Heimann, H. Neddermeyer, and H.F. Roloff, J. Phys. C **10**, L17 (1977).
[4] A. Zangwill *Physics at Surfaces* (Cambridge University Press, Cambridge, 1988).
[5] N. W. Ashcroft and N. D. Mermin, *Solid State Physics* (Saunders, Philadelphia, 1976).
[6] S.-Å. Lindgren and L. Walldén, Solid State Commun. **34**, 671 (1980).
[7] S.-Å. Lindgren and L. Walldén, Phys. Rev. Lett. **59**, 3003 (1987).
[8] A. Carlsson, B. Hellsing, S.-Å. Lindgren, and L. Walldén, Phys. Rev. B **56**, 1593 (1997).
[9] R. Dudde, L.S.O. Johansson, and B. Reihl, Phys. Rev. B **44**, 1198 (1991).
[10] N. Fischer, S. Schuppler, R. Fischer, Th. Fauster, and W. Steinmann, Phys. Rev. B **43**, 14 722 (1991).
[11] J. Kliewer, R. Berndt, E.V. Chulkov, V.M. Silkin, P.M. Echenique, and S. Crampin, Science **288**, 1399 (2000).
[12] J.M. Carlsson and B. Hellsing, Phys. Rev. B **61**, 13 973 (2000).
[13] B. Hellsing, J. Carlsson, L. Walldén, and S.-Å. Lindgren, Phys. Rev. B **61**, 2343 (2000).
[14] N. Memmel and E. Bertel, Phys. Rev. Lett. **75**, 485 (1995).
[15] E. Bertel, P. Roos, and J. Lehmann, Phys. Rev. B **52**, R14 384 (1995).
[16] J.V. Lauritsen, S. Helveg, E. Lægsgaard, I. Stengaard, B.S. Clausen, H. Topsø, and F. Besenbacher, J. Catal. **197**, 1 (2001).
[17] S.J. Stranick, M.M. Kamna, and P.S. Weiss, Science **266**, 99 (1994).
[18] E. Bertel, Phys. Status Solidi A **159**, 235 (1997).
[19] M.F. Crommie, C.P. Lutz, and D.M. Eigler, Science **262**, 218 (1993).
[20] H. Roder, E. Hahn, H. Brune, J.-P. Bucher, and K. Kern, Nature (London) **366**, 141 (1993).
[21] E. Wimmer, J. Phys. F: Met. Phys. **13**, 2313 (1983).
[22] V. Lindberg and B. Hellsing, Surf. Sci. **506**, 297 (2002).
[23] N. D. Lang, in *Theory of the Inhomogeneous Electron Gas*, edited by S. Lundqvist and N. H. March (Plenum, New York, 1983), p. 309.
[24] R.O. Jones and O. Gunnarsson, Rev. Mod. Phys. **61**, 689 (1989).
[25] T. Torsti, M. Heiskanen, M. J. Puska, and R. M. Nieminen, Int. J. Quantum Chem., (to be published); e-print cond-mat/0205056.
[26] M. Heiskanen, T. Torsti, M.J. Puska, and R.M. Nieminen, Phys. Rev. B **63**, 245106 (2001).
[27] For a short review and a promising new idea, see the recent paper by D. Raczkowski, A. Canning, and L.W. Wang, Phys. Rev. B **64**, 121101 (2001).
[28] F.K. Schulte, Surf. Sci. **55**, 427 (1976).
[29] M. Manninen, R.M. Nieminen, P. Hautojärvi, and J. Arponen, Phys. Rev. B **12**, 4012 (1975).
[30] W.A. de Heer, Rev. Mod. Phys. **65**, 611 (1993); M. Brack, *ibid.* **65**, 677 (1993).
[31] N. Zabala, M.J. Puska, and R.M. Nieminen, Phys. Rev. Lett. **80**, 3336 (1998).
[32] N. Zabala, M.J. Puska, and R.M. Nieminen, Phys. Rev. B **59**, 12 652 (1999).
[33] M.J. Puska, E. Ogando, and N. Zabala, Phys. Rev. B **64**, 033401 (2001).
[34] R. Diehl and R. McGrath, Surf. Sci. Rep. **23**, 43 (1996).
[35] D. Tang, D. McIlroy, X. Shi, C. Su, and D. Heskett, Surf. Sci. Lett. **255**, L497 (1991).
[36] S.-Å. Lindgren and L. Walldén, Phys. Rev. B **38**, 3060 (1988).

[37] J. Kliewer and R. Berndt, Surf. Sci. **477**, 250 (2001).
[38] J. Kliewer and R. Berndt, Phys. Rev. B **65**, 035412 (2001).
[39] A. Carlsson, S.-Å. Lindgren, C. Svensson, and L. Walldén, Phys. Rev. B **50**, 8926 (1994).
[40] J. Li, W.-D. Schneider, R. Berndt, and S. Crampin, Phys. Rev. Lett. **80**, 3332 (1998).
[41] J. Li, W.-D. Schneider, S. Crampin, and R. Berndt, Surf. Sci. **422**, 95 (1999).
[42] J. Kliewer and R. Berndt, Appl. Phys. A: Mater. Sci. Process. **A72**, S155 (2001).
[43] A. Brandt, Math. Comput. **31**, 333 (1977).
[44] C. Kittel, *Introduction to Solid State Physics*, 7th ed. (Wiley, New York, 1996), pp. 248–252.
[45] G. Makov, R. Shah, and M.C. Payne, Phys. Rev. B **53**, 15 513 (1996); T. Korhonen, M.J. Puska, and R.M. Nieminen, *ibid.* **54**, 15 016 (1996).
[46] G. Binnig and H. Rohrer, Helv. Phys. Acta **55**, 726 (1982).
[47] J. Tersoff and D.R. Hamann, Phys. Rev. B **31**, 805 (1985).
[48] A. Selloni, P. Carnevali, E. Tosatti, and C.D. Chen, Phys. Rev. B **31**, 2602 (1985).
[49] D.M. Ceperley and B.J. Alder, Phys. Rev. Lett. **45**, 566 (1980); J.P. Perdew and A. Zunger, Phys. Rev. B **23**, 5048 (1981).
[50] J. Li, W.-D. Schneider, and R. Berndt, Phys. Rev. B **56**, 7656 (1997).